Journal of Water Process Engineering 42 (2021) 102120

Contents lists available at ScienceDirect

Journal of Water Process Engineering

journal homepage: www.elsevier.com/locate/jwpe

Synergetic effects of dodecylamine-functionalized graphene oxide nanoparticles on antifouling and antibacterial properties of polysulfone ultrafiltration membranes

Abedalkader Alkhouzaam, Hazim Qiblawey *

Department of Chemical Engineering, College of Engineering, Qatar University, P. O. Box 2713, Doha, Qatar

ARTICLE INFO

Keywords:
Dodecylamine
Graphene oxide
Ultrafiltration
Antifouling
Antibacterial effect

ABSTRACT

The potential use of dodecylamine-functionalized graphene oxide (rGO-DDA) nanoparticles as an antifoulant and antibacterial nanofiller was investigated. GO and rGO-DDA were analyzed using Raman spectroscopy, FTIR, SEM, TEM, and TGA that all confirmed the successful functionalization of GO structure. Polysulfone (PSF) ultrafiltration membranes incorporating varied loadings of GO and rGO-DDA were then fabricated via phase inversion approach. All membranes were characterized in terms of chemical structure, morphology, hydrophilicity, porosity and mean pore size. Cross-section SEM images showed the distribution of GO and rGO-DDA between the pores and on the polymer walls. AFM results demonstrated that GO addition increased the roughness of membrane; while with rGO-DDA addition the surface became smoother. Pristine PSF and rGO-DDA based membranes exhibited similar hydrophilicity, while GO-based membranes exhibited higher hydrophilicity as revealed by contact angle measurements. Permeability, separation and antifouling experiments were performed in a cross-flow membrane setup and showed that flux decreases with the increase in GO and rGO-DDA concentration. rGO-DDA membranes showed higher antifouling and antibacterial performance compared to the pristine PSF and GO membranes. Neat PSF exhibited 65.4 % flux recovery ratio (FRR) against BSA that was increased to 86.9 % and 89.1 % with GO-0.1 and rGO-DDA-0.1, respectively. Against HA, FRR was improved from 87.8 % for neat PSF to 95.6 % and 99.3 % with GO-0.1 and rGO-DDA-0.1, respectively. Additionally, rGO-DDA membrane exhibited higher bacteriostatis rate (83.6 %) against *H. aquamarina* than GO membrane (62.9 %). Moreover, rGO-DDA nanoparticles exhibited excellent dispersibility in several solvents making them promising nanofillers for various membranes with high antifouling and antibacterial performance.

1. Introduction

Amongst the several technologies evolved in water treatment and purification sector, membrane-based processes are considered promising solution to afford clean water [1]. It is considered efficient and economical due to the low energy consumption, small footprint, and the relatively low cost compared to other technologies [2]. Several membrane-based processes have been arisen to meet the various needs in water treatment sector including microfiltration (MF), ultrafiltration (UF), nanofiltration (NF), reverse osmosis (RO), and forward osmosis (FO). Among them, UF is a fast-growing technology that has demonstrated a remarkable contribution to water treatment sector. Because of its capability to separate a wide range of impurities from water at low cost, it is considered an efficient and economical pre-treatment process for NF and RO [3]. UF can separate proteins, turbidity, viruses, bacteria and various organic matters from wastewater in a safe, clean and efficient way. The utilization of UF membranes is not only limited to water treatment but also it showed an increasing interest in chemical recovery, dairy production, food industry, pharmaceutical applications, and textile industry and paint treatment [4,5]. Despite of the several advantages of membranes, their susceptibility to fouling is still a bottleneck issue in many applications. Fouling is a phenomenon where pollutants in the wastewater accumulate onto the membrane surface and block the pores resulting in a decline in the membrane performance and shortage in its service life [6]. Hence, investigating new methods, materials, and fillers became the focus of most studies aiming to produce high-efficient membranes with high fouling resistance.

The use of nanomaterials as membrane fillers is one of the well-

* Corresponding author.
E-mail address: hazim@qu.edu.qa (H. Qiblawey).

https://doi.org/10.1016/j.jwpe.2021.102120
Received 2 March 2021; Received in revised form 12 April 2021; Accepted 28 April 2021
Available online 6 May 2021

established methods being developed in membrane sector [7]. The addition of nanofillers can improve membrane performance and properties like antifouling, antibacterial activity, flux, and rejection [8]. Various nanomaterials have been investigated as membrane nanofillers and exhibited high performance such as carbon nanotubes (CNTs) [9], zeolites [10], metal organic frame works (MOFs) [11], graphene-based materials [12,13], SiO_2 [14], MXene [15], TiO_2 [16], etc. Among them, graphene oxide (GO) and GO-based materials attracted remarkable research interest in the past few years due to their stability, tuneability, mechanical strength, and easy accessibility [17]. Furthermore, GO-based materials exhibit high fouling resistance and bactericidal effects against various foulants and bacteria making them promising nanofillers to produce high antifouling membranes [18,19]. Additionally, the oxygen content in the functional groups (e.g. hydroxyls, carboxyls, ketones and epoxides) existing on the GO sheets edges enriches GO hydrophilicity and make it a versatile platform for further functionalization to derive other graphene-based materials to meet different purposes [20,21]. Furthermore, GO can be easily exfoliated in various polymer matrices and polar aprotic solvents [22] which makes it a good candidate to be utilized as nanofiller in membranes fabrication sector.

The efficient utilization of nanofillers in membranes fabrication depends on the better interfacial interaction between polymeric matrix and the nanofiller as well as the uniform and stable dispersion in the matrix [23]. However, pristine nanoparticles (e.g. CNTs, GO, etc.) cannot achieve stable and uniform dispersion which limits the efficiency of using them as fillers in some polymer matrices [24]. Therefore, several studies investigated the effect of functionalization on the properties of nanoparticles as well as on the overall membrane performance. Studies reported that a successful functionalization could significantly enhance GO properties to fit different purposes and applications. For example, GO functionalization with hydrophobic materials like octadecylamine (ODA) [25] and n-butylamine (NBA) [26] enhances the performance in membrane distillation (MD) processes where the membrane hydrophobicity is preferable. In contrast, GO functionalization with hydrophilic materials, like polydopamine (PDA) [27], polyvinylpyrrolidone (PVP) [28], and starch [29], enhances the performance in membrane processes where the hydrophilicity is desirable (e.g. UF, NF, RO, etc.). Several studies have been conducted in literature on the functionalization of GO for different membrane-based water treatment processes including FO, RO, NF and UF. Safarpour et al. [30,31] studied the effect of GO functionalization with TiO_2 on RO and NF membranes and reported a clear improvement of fouling resistance. Rajakumaran et al. [32] prepared RO membranes by incorporating amino-functionalized zinc oxide (ZnO) and GO composites (GO-ZnO) into the thin-film-nanocomposite layer (TFN) and reported better antifouling performance compared to pristine membrane. Zhang et al. [33] have recently reported that modifying GO with p-aminophenol enhanced the antibacterial of RO membranes significantly when compared to GO—RO and pristine RO membranes. Similar studies investigated the effect of GO functionalization with various functional groups on the fouling resistance of UF membranes and showed clear improvement against various foulants. Functional materials used to functionalize GO include isocyanate [34], hyperbranched polyethyleneimine (HPEI) [35], cysteine [36], guanidyl [37], polydopamine (PDA) [27]. Among the various functional groups investigated in the functionalization of GO nanosheets, amines are considered promising agents that can enhance GO properties as well as the overall membrane performance. The amination of GO nanosheets is not novel and was investigated in different studies using various amines. For example, the amination of GO with HPEI could improve the interactions between the nanofiller (e.g. GO-HPEI) and the polymer matrix which enhanced the mechanical properties of polyethersulfone (PES) membrane [35]. In a previous work, we demonstrated that the GO amination with PDA could enhance the flux and the fouling resistance without compromising the rejection performance [27]. Similar observation has been also reported with 3-aminopropyl triethoxysilane (APTS)-aminated GO that showed significant enhancement of the sulfonated-PES performance in terms of flux and organic fouling resistance [38]. Moreover, amine-functionalization of GO nanosheets was found to enhance the membrane's antibacterial activity [35,39]. In this context, dodecylamine (DDA), a cationic surfactant, can be a promising functionalizing agent that enhances GO properties in terms of fouling resistance and antibacterial activity. DDA was previously used to functionalize multi-walled carbon nanotubes (MWCNTs) and exhibited ~46 % antifouling enhancement against proteins [40]. Additionally, studies reported that DDA has strong bactericidal effects against several bacteria [41]. DDA can also promote the formation of alkyl group on the edges of GO nanosheets providing better dispersibility of GO in non-polar solvents and a better distribution within the polymer matrix [42]. The higher dispersibility of GO nanosheets in the solvent leads to a better distribution and interactions of GO with the polymer matrix.

In this work, amine-functionalized GO nanoparticles were prepared and used as nanofiller in UF polysulfone (PSF) composite membranes. The amination of GO was carried out using the direct functionalization of GO nanosheets with DDA via a simple temperature-assisted reflux method. We aim through this study to investigate the synergetic effects of GO and DDA on the antifouling properties and the bactericidal activity of PSF composite membranes. Pristine GO and rGO-DDA nanosheets were incorporated into PSF via the non-solvent induced phase separation technique (NIPS) at low concentrations (0−0.15 wt.%). The dynamic fouling resistance of the fabricated membranes was investigated against organic and protein fouling represented by humic acid (HA) and Bovine Serum Albumin (BSA), respectively. The antibacterial activity of the prepared membranes against *Halomonas aquamarina* (*H. aquamarina*) as the model bacterium was studied using bacteriostasis rate determination approach. The effect of GO and rGO-DDA incorporation on the PSF morphology, hydrophilicity, permeability and separation efficiency was investigated, too. Moreover, the structural and spectral properties of GO and rGO-DDA were studied.

2. Experimental details

2.1. Materials

Graphite (Gr) flakes (99.9 %, -10 mesh) were supplied by Alfa Aesar. Potassium permanganate ($KMnO_4$,99 %), sulfuric acid (H_2SO_4, 95 %), polyvinylpyrrolidone (PVP, ≥ 95 %), toluene (≥ 99.5 %) were procured from Fisher Scientific. Hydrogen peroxide (H_2O_2, 30 %), hydrochloric acid (HCl, 35–38%), phosphoric acid (H_3PO_4, 99 %), and, hexane (≥ 98.5 %) were procured from BDH. Dodecylamine (DDA, > 97 %), polysulfone pellets (PSF, Mw ~ 35,000), Bovine Serum Albumin (BSA, ≥ 96 %, Mw ~ 66 kDa), *N,N*-Dimethylacetamide (DMAc, ≥ 99 %), 1-Methyl-2-pyrrolidinone (NMP, 99.5 %), ethanol (≥ 99.8 %), and humic acid (HA) were obtained from Sigma Aldrich. *N,N*-Dimethylformamide (DMF, ≥ 99.8 %) and dodecane (≥ 99 %) were purchased from Honeywell. All chemicals were used as purchased without further purification.

2.2. Preparation and functionalization of GO nanoparticles

GO nanoparticles were synthesized via a modified Hummers method that was previously reported [43]. In brief, a mixture of 24 mL of H_2SO_4 and 6 mL of H_3PO_4 was stirred in an ice bath for several minutes. 1 g of Gr flakes and 3 g of $KMnO_4$ were then added into mixing solution under the same conditions. The reactants were then stirred at 95 ± 2 °C in an oil bath for 30 min followed by the addition of 50 mL deionized water (DI) and stirring for another 30 min at the same conditions. The reaction was then terminated by adding DI (150 mL) and H_2O_2 (20 mL). The mixture was then diluted with HCl (20 %) and centrifuged, followed by several washing/centrifugation cycles with DI until obtaining a neutral pH. GO nanoparticles were then obtained by drying the samples overnight at 80 °C.

The dried GO nanoparticles were then aminated with DDA using the temperature-assisted solution interaction technique [23]. In brief, 100 mg of GO were dispersed in DI (50 mL) and 300 mg of DDA were dispersed in ethanol (50 mL) and both solutions were then ultra-sonicated for 1 h. Both GO and DDA suspensions were mixed in a round bottom flask and stirred in an oil bath (60 °C, 48 h) under the reflux conditions. The aminated GO (rGO-DDA) nanoparticles were then obtained by the solvent evaporation technique followed by several washings with ethanol followed by vacuum drying at 85 °C overnight. A schematic representation of the GO synthesis, the amination reaction with DDA and the anticipated structure of rGO-DDA is presented in Fig. 1.

2.3. Membranes preparation

Bare PSF, PSF/GO and PSF/rGO-DDA mixed matrix membranes (MMMs) were prepared using the well-known non-solvent induced phase separation method [44]. In brief, PSF (17 wt.%) in NMP was used as the main casting solution with 3 wt.% PVP as the pore former. For the preparation of PSF/GO and PSF/rGO-DDA casting solutions, two stock dispersions (0.5 mg/mL) of the pristine GO and rGO-DDA in NMP were prepared and sonicated for 2 h. Different loadings of GO and rGO-DDA were then added to NMP according to Table 1. PSF and PVP were then slowly added to the dispersions and stirred vigorously for 2 h followed by slow stirring overnight until homogenous solutions were obtained (Figure S1 in the supplementary information). The obtained solutions were then casted on a clean glass plate at a uniform speed using an automated casting machine equipped with a film applicator (Elcometer ®, UK). The casted solutions were then soaked into a coagulant bath (DI) where the phase inversion took place and the membrane detached freely from the glass plate. The obtained membranes were then washed and kept in DI for until testing. Fig. 2 illustrates the phase inversion technique for the fabrication of membranes studied in this work. The compositions and codes of the prepared membranes are presented in Table 1.

2.4. Nanoparticles characterization

The properties of the synthesized GO and rGO-DDA nanoparticles were analyzed using different characterization techniques to investigate the contribution of oxidation conditions as well as the functionalization reaction to the properties of both samples. The elemental compositions were obtained by the CHNSO elemental analyzer (Flash 2000, Thermo Scientific™). FTIR spectra were recorded using Perkin Elmer 2000 FTIR-UATR spectrometer in the range of 400 – 4000 cm^{-1}. DXR Raman Spectrometer with a 532 nm laser and a 10× objective (Thermo Scientific) was used to obtain Raman spectra at room temperature. The morphological structures of GO and rGO-DDA were evaluated using the transmission electron microscopy (TEM) with FEI Tecnai F20 (200 kV) and scanning electron microscopy (SEM) using JEOL model JSM-6390LV. Moreover, the thermal stability of both nanoparticles was analyzed using the Thermogravimetric analysis (TGA) with a PerkinElmer thermogravimetric analyzer (Pyris 6 TGA) at a heating rate of 10 °C/min, temperature range of 30−800 °C, and under nitrogen.

Table 1
Notations and compositions of the PSF, PSF/GO, and PSF/rGO-DDA MMMs.

Membrane	PSF (g)	PVP (g)	NMP (mL)	Stock dispersion (mL)	GO (wt. %)*	rGO-DDA (wt. %)*
PSF	5.53	0.975	25	0	–	–
GO-0.02	5.53	0.975	23	2 (GO)	0.02	–
GO-0.05	5.53	0.975	20	5 (GO)	0.05	–
GO-0.1	5.53	0.975	14	11 (GO)	0.1	–
GO-0.15	5.53	0.975	8	17 (GO)	0.15	–
rGO-DDA-0.02	5.53	0.975	23	2 (rGO-DDA)	–	0.02
rGO-DDA-0.05	5.53	0.975	20	5 (rGO-DDA)	–	0.05
rGO-DDA-0.1	5.53	0.975	14	11 (rGO-DDA)	–	0.1
rGO-DDA-0.15	5.53	0.975	8	17 (rGO-DDA)	–	0.15

* GO and rGO-DDA compositions are with respect to PSF weight.

2.5. Dispersion studies of GO and rGO-DDA

The dispersibility of GO and rGO-DDA nanoparticles was investigated in DI and various organic solvents including dodecane, hexane, toluene, NMP, DMF, and DMAc. The dispersibility measurements were conducted with a concentration of 0.5 mg/mL in an ultrasonic bath sonicator at room temperature for 2 h.

2.6. Membranes characterization

To investigate the effect of GO incorporation into the PSF matrix, the prepared membranes were characterized using FTIR-UATR (Perkin Elmer 2000). Surface and cross-section SEM images at different magnifications were obtained using (JEOL model JSM-6390LV). The preparation of cross-section samples was done by freezing the membrane samples in liquid nitrogen and then fracturing them to prevent the deformation of the membranes structure [45,46]. The surface roughness of the prepared membranes in terms of the root-mean-square roughness (RMS) and average roughness (Ra) were evaluated using the Atomic force microscopy (AFM-MFP-3D) from Asylum Research, US. AFM images were obtained over a scan area of 5 × 5 μm with 1 Hz scan rate. Membranes hydrophilicity in terms of water contact angle (CA) was

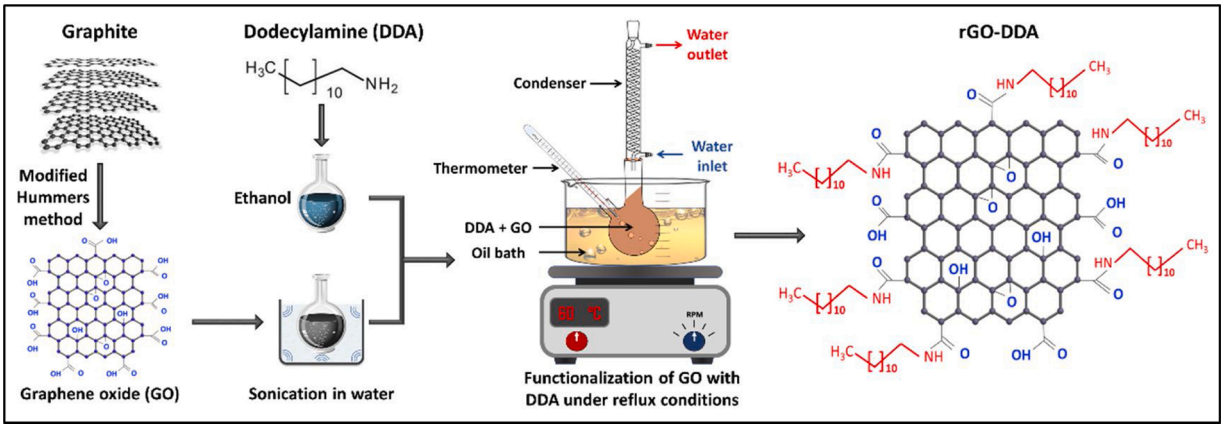

Fig. 1. Schematic representation of the functionalization reaction of GO with DDA.

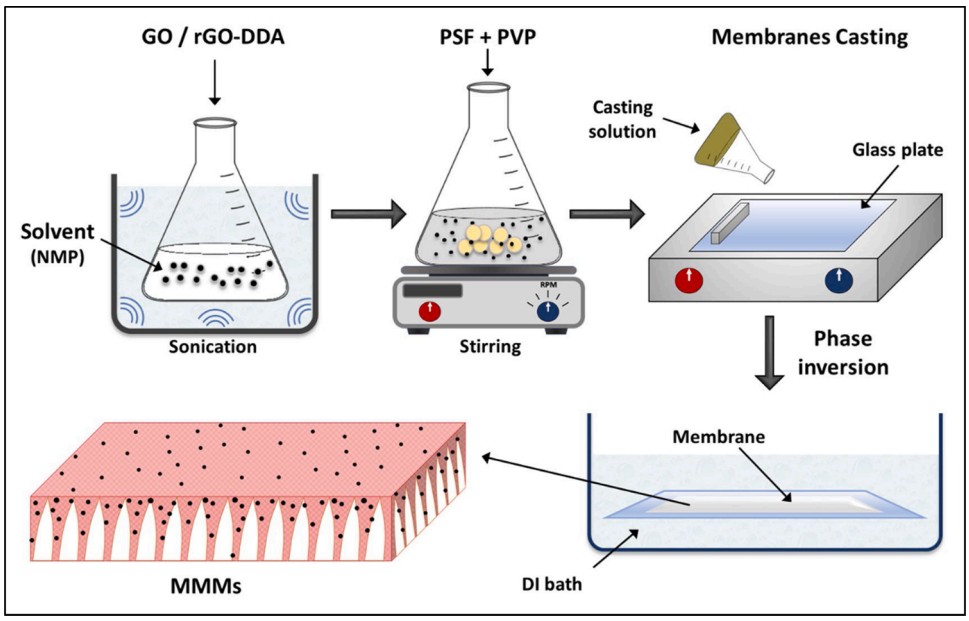

Fig. 2. illustration of the GO based MMMs preparation using phase inversion technique.

measured with a DataPhysics contact angle analyzer (OCA15 Pro, Germany). The CA measurements were conducted using DI droplets of 2 μm at minimum of 15 points of each membrane.

Membranes porosity measurements were carried out using the gravimetric method. two Circular samples of the prepared membranes were obtained using a circular cutter with a fixed cutting area of 12.6 cm^2. The samples were then kept in DI overnight at room temperature, excess water was then carefully mopped with a tissue paper and weighted immediately (w_w). The samples were dried overnight and the dry membrane weight (w_d) was then recorded. The membrane porosity was then estimated using Eq. 1 [27,47] :

$$\varepsilon = \frac{w_w - w_d}{A \times l \times \rho_w} \tag{1}$$

Where A (cm^2) is the effective membrane area, l (cm) is the membrane thickness determined from the cross-section SEM images, and ρ_w is the density of water at 23 °C (0.998 g/cm^3). Guerout-Elford-Ferry equation (Eq. 2) was used to estimate the mean pore size (r_m) of the prepared membranes [48]:

$$r_m = \sqrt{\frac{(2.9 - 1.75\varepsilon) \times 8\eta l Q}{\varepsilon \times A \times \Delta P}} \tag{2}$$

Where ΔP (Pa) is the operational pressure, Q (m^3/s) is the volumetric flow rate of the permeate, and η is the viscosity of water at 23 °C (9.3×10^{-4} Pa.s)

2.7. Permeability, rejection, and antifouling measurements

Pure water flux, rejection and dynamic fouling measurements were performed using a cross-flow membrane unit obtained from (Sterlitech Corp, US). The feed tank is equipped with a cooling/heating water circulator to control the feed temperature. Fig. 3 illustrates the process flow diagram of the membrane unit used in this work. All filtration experiments were performed at 1 bar, 46.1 ± 0.3 cm.s^{-1} cross-flow velocity and a temperature of 23 ± 0.5 °C. Briefly, the membrane was firstly compacted with DI for 30 min at 4 bar. The pressure was then reduced to 1 bar and kept for additional 30 min to ensure a stable flux. The pure water flux (J_{w0}, LMH) and permeability (PWP, LMH/bar) of

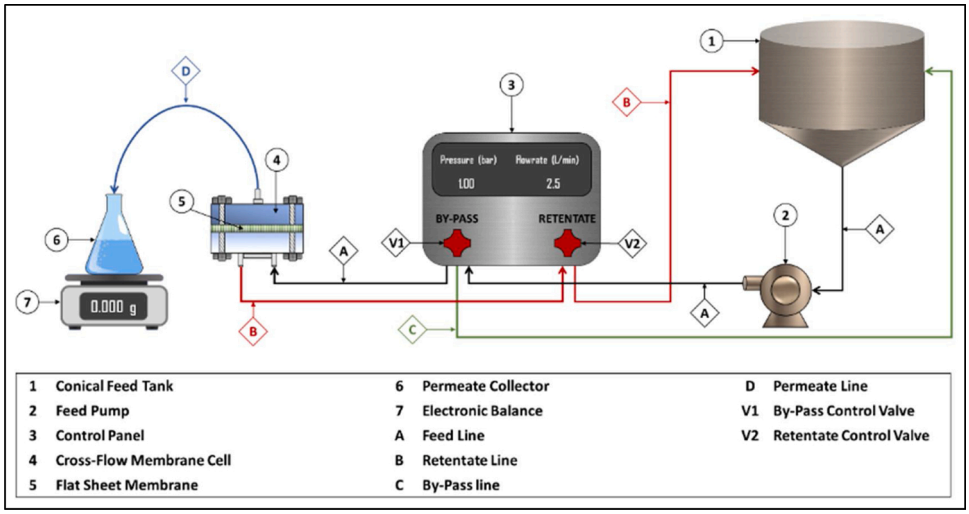

Fig. 3. Process flow diagram of the cross-flow membrane unit.

membranes were then calculated using Eqs. (3) and (4), respectively [49].

$$J = \frac{V}{A.t} \tag{3}$$

$$PWP = \frac{Q}{\Delta P.A} \tag{4}$$

Where V (L) is the volume of permeate, t (h) is the sampling time, A (m^2) is the effective filtration area, Q (L/h) is the volumetric flow rate of permeate, and ΔP (bar) is the trans-membrane pressure difference.

The rejection and antifouling experiments were then conducted by shifting the feed to freshly prepared solutions of HA (25 mg/L) and BSA (500 mg/L) as model organic and protein foulants, respectively. After 1 h filtration time, the foulant flux (J_{wf}) and rejection (R%) were then calculated according to Eqs. 3 and 5, respectively.

$$R(\%) = \left(1 - \frac{C_p}{C_f}\right) \times 100 \tag{5}$$

Where C_f and C_p are the foulant concentrations in the feed and permeate, respectively. HA and BSA concentrations were measured at 254 nm [47,50], and 278 nm [51,52], respectively, with a UV–vis spectrophotometer (UV-2700, Shimadzu, Japan). After foulants filtration, the feed was shifted back to DI for membrane washing. Three washing cycles (10 min each) were performed without an applied pressure at 46.1 ± 0.3 $cm.s^{-1}$ cross-flow velocity. The steady PWF (J_{w1}) was then recorded at 1 bar and the same cross-flow velocity. The flux recovery ratio (FRR%), total fouling ratio (R_t%), irreversible fouling ratio (R_{ir}%) and reversible fouling ratio (R_r%) were then calculated by Eqs. 6 to 9, respectively [53,54]:

$$FRR(\%) = \frac{J_{w1}}{J_{w0}} \times 100 \tag{6}$$

$$R_t(\%) = \frac{J_{w0} - J_{wf}}{J_{w0}} \times 100 \tag{7}$$

$$R_{ir}(\%) = \frac{J_{w0} - J_{w1}}{J_{w0}} \times 100 \tag{8}$$

$$R_r(\%) = \frac{J_{w1} - J_{wf}}{J_{w0}} \times 100 \tag{9}$$

2.8. Antibacterial activity measurements

The antibacterial properties of the pristine PSF and composite membranes were evaluated by the bacteriostasis rate determination method [35,55]. *H. aquamarina* were used as the model bacterium. 16 mg of the PSF, PSF/GO and PSF/rGO-DDA were cut and washed with ethanol then with DI to remove ethanol residuals. Membrane samples were then added to 10 mL of Luria Bertani (LB) solution incubated with appropriate volume of *Halomonas* to obtain initial optical density of 0.1 at 600 nm (OD600). Samples were then incubated at 30 °C for 18 h after which they were removed from cultures and rinsed with saline. The serial dilution technique was employed to get the actual number of cells at the beginning and the end of experiment (t = 0 and t = 18 h). The number of colonies on each plate was determined using the counting method. Bacteristasis rate (BR%) was then calculated using Eq. 10:

$$BR(\%) = \frac{n_0 - n_1}{n_0} \times 100\% \tag{10}$$

Where n_0 and n_1 represent the number of colonies on the plates treated with the control membrane (e.g. pristine PSF) and plates treated with the hybrid membranes (e.g. PSF/GO and PSF/rGO-DDA), respectively.

3. Results and discussion

3.1. Nanoparticles characterization

The FTIR-UATR spectra of DDA, pristine GO, and rGO-DDA are presented in Fig. 4a. The graphite oxidation can be confirmed by the presence of different bands related to the oxygenated functional groups in the spectra of pristine GO. These bands were previously reported with GO nanoparticles [43,56]. Fig. 4a confirms also the successful functionalization of GO with DDA by the emergence of different bands. The two bands around 2917 and 2849 cm^{-1} correspond to C–H stretching vibration [57]. Moreover, the formation of amide-carbonyl bonds between DDA and GO sheets is confirmed by the presence of N—H amide bending and CN— amide stretching at ~1546 and 1464 cm^{-1}, respectively [58]. The spectra also show that the C═O band at ~ 1707 cm^{-1} was reduced with the rGO-DDA due to the reduction of the oxygen along with the alkyl chain addition to the GO structure [22]. Fig. 4b shows the Raman spectra of the pristine GO and rGO-DDA and confirms the GO formation through the presence of D and G bands, that are characteristic for GO-based materials [43]. It has been reported in various studies that the intensities ratio of D and G bands (I_D/I_G) is related to the crystallite properties of GO [59,60]. The I_D/I_G ratio for the pristine GO and rGO-DDA were estimated from the spectra deconvolution and fitting and were found to be 1.8 and 2.1, respectively, indicating an obvious change in the crystallite structure caused by the functionalization reaction with DDA. The increase in the I_D/I_G ratio can be attributed to the formation of sp^3 carbon within the sp^2 carbon network of graphene [57]. The deconvolution and fitting of Raman spectra as well as the bands parameters are presented in Figure S2 and Table S1 in the supplementary information, respectively. The Elemental analysis results (Table 2) shows good degree of graphite oxidation represented by the high oxygen content and O/C ratio (50 % and 1.1, respectively). However, the functionalization with DDA reduced the GO oxygen content to 12.3 wt. % and increased C, N and H compositions to 77.4, 3.8 and 6.5 wt.%, respectively, due to the addition of the alkyl chain which agrees with the findings of the FTIR analysis.

The SEM images shown in Fig. 5a show clear difference in the morphology of GO and rGO-DDA nanoparticles. The pristine GO nanoparticles exhibit clear, sharp and smooth surface, while rGO-DDA showed irregular structure and high roughness. This observation has been reported with different amine-functionalized GO nanoparticles

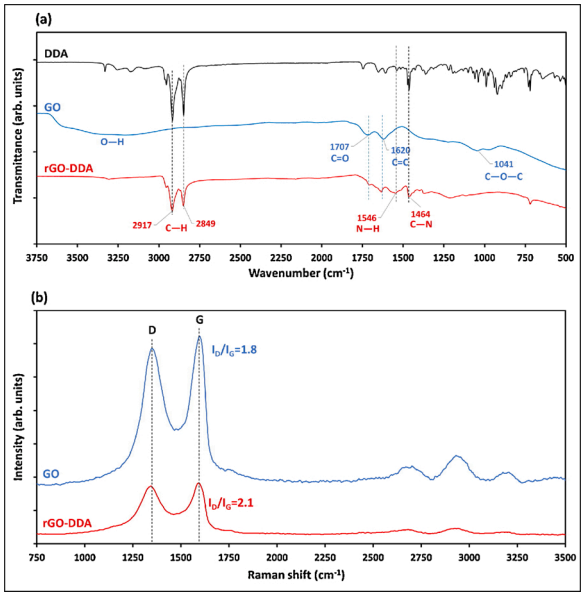

Fig. 4. (a) FTIR-UATR spectra and (b) Raman spectra of the pristine GO and rGO-DDA nanoparticles.

Table 2
Elemental compositions of the prepared GO and rGO-DDA.

Sample	Elemental analysis (wt.%)					O/C
	N%	C%	H%	S%	O%	
GO	0.3	46.8	2.6	0.3	50.0	1.1
rGO-DDA	3.8	77.4	6.5	0.0	12.3	0.2

[23,25,61] and can be explained by the intercalation and attachment of DDA molecules between GO sheets. The different morphological structure can be also confirmed by the TEM images shown in Fig. 5b. The pristine GO sheets exhibit wrinkled surface with high transparency indicating a low stacking level and high oxidation degree of GO nanoparticles [43,56]. On the other hand, rGO-DDA exhibits opaque and dense surfaces caused by the GO reduction which cause an increase in the staking level of GO sheets. Similar observations were reported with the functionalization of GO with different amines such as PDA [61], ODA [62], p-phenylenediamine (PPD) and hexamethylene diamine (HMD) [63]. The thermal stability of GO and rGO-DDA nanoparticles was investigated using the TGA analysis. The TGA curves shown in Figure S3 in the supplementary information suggest different thermal stabilities of GO and rGO-DDA nanoparticles which is mainly attributed to the difference of their elemental compositions [43]. The TGA curve of pristine GO shows a slight weight reduction around 100 °C attributed to the evaporation of water molecules between the GO nanosheets. However, no weight loss was observed before 100 °C with rGO-DDA which indicates a hydrophobic nature of rGO-DDA that resists water to be attached to its surface during functionalization. Both GO and rGO-DDA exhibited a major weight loss around 243 °C and 307 °C. The major loss in this temperature range is usually attributed to the thermal degradation of oxygenated functional groups of GO [64]. The oxygenated groups of GO sheets were reduced when functionalized with DDA as revealed by the FTIR and the elemental analysis. Therefore, the major weight loss with rGO-DDA nanoparticles occurred at higher temperature compared to the pristine GO. In summary, all characterization techniques confirm the successful functionalization and incorporation of DDA molecules on the surface and between GO sheets.

3.2. *Dispersion studies of GO and rGO-DDA*

Photographs of GO and rGO-DDA dispersions just after sonication are shown in Fig. 6. GO showed good degree of dispersion in DI, DMF, DMA and NMP. However, in dodecane, toluene and hexane, the dispersion was very poor which agrees with other studies in the literature [23,61].

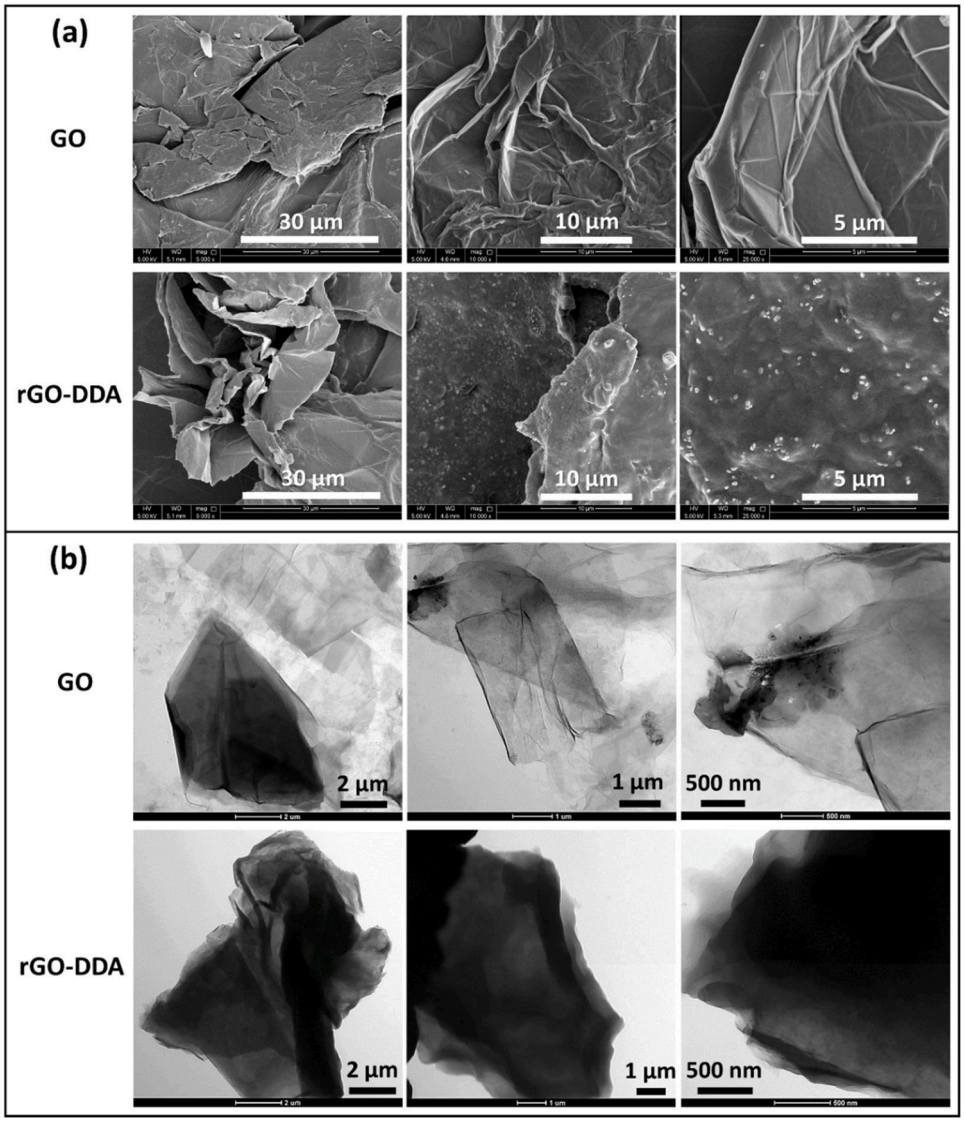

Fig. 5. (a) SEM and (b) TEM images of GO and rGO-DDA nanoparticles at different magnifications.

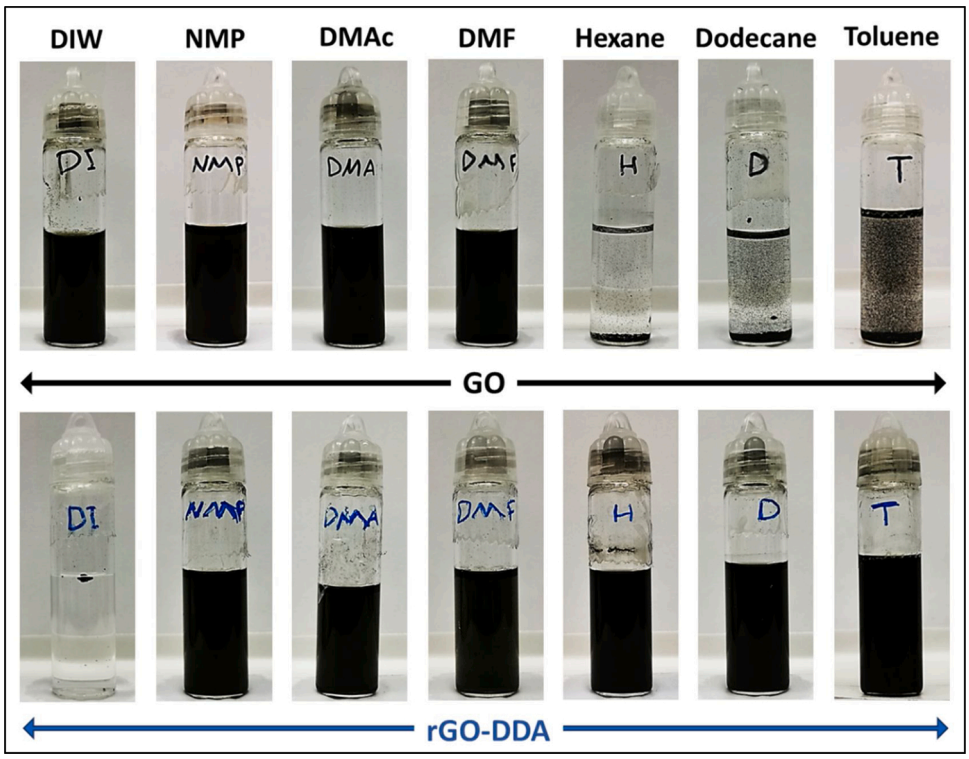

Fig. 6. Photographs of GO and rGO-DDA dispersions in water and different organic solvents.

In comparison, rGO-DDA exhibited higher dispersibility in all solvents except in DI. The poor dispersion of rGO-DDA in DI can be related to the reduction of the oxygen along with the alkyl chain addition to the GO structure [22] which reduces the hydrophilicity of GO sheets. The good dispersion of rGO-DDA in other solvents allows it utilization as membrane filler with various types of polymers (PSF, PVDF, PES, PAN, etc.) and for different applications (UF, NF, FO and RO). However, the limited dispersion properties of the raw GO restrict its usage for such applications [24].

3.3. Membranes characterization

3.3.1. FTIR-UATR spectra

FTIR-UATR spectra of the control PSF, PSF/GO and PSF/rGO-DDA composite membranes are presented in Fig. 7. The PSF characteristic bands are presented in all spectra around 1664, 1320, 1291, 1241, 1150, 1108 cm^{-1} corresponding to aromatic ring breathing, O—SO— asymmetric stretching, S═O stretching, COC stretching, OSO——— symmetric stretching, and S═O stretching. The two bands around 1586 and 1487 cm^{-1} correspond to the aromatic ring stretching. These bands have been previously reported with PSF membranes [65,66]. The spectra of the composite membranes are almost identical to this of the pristine PSF and depict no difference which can be related to the dominance of PSF and the low concentrations of nanofillers in the polymer matrix [67].

3.3.2. Morphology (SEM & AFM)

Surface and cross-section SEM were studied at various magnifications to investigate the influence of GO and rGO-DDA incorporation on PSF morphological structure. Figs. 8 and 9 show the obtained SEM images with different concentrations of GO and rGO-DDA, respectively. In the surface SEM images, no clear difference between the bare PSF, PSF/GO and PSF/rGO-DDA can be observed. On the other hand, clear influence of GO and rGO-DDA addition on PSF structure can be observed from the cross-section SEM images. All membranes showed two distinct layers: a top layer with a semi-dense structure and a sublayer with a

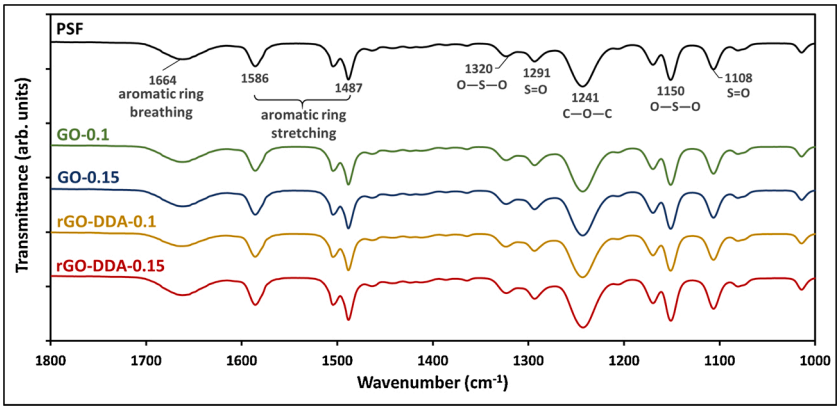

Fig. 7. FTIR-UATR spectra of PSF, PSF/GO and PSF/rGO-DDA MMMs.

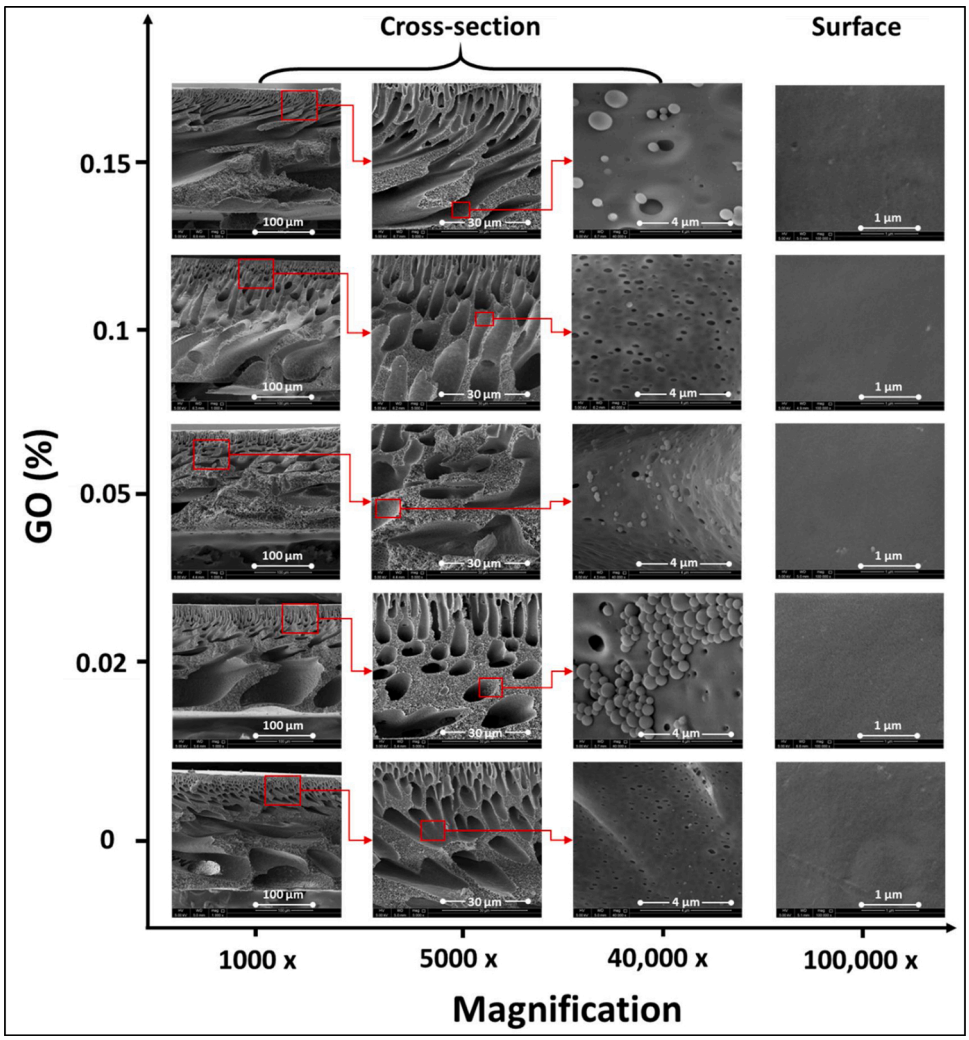

Fig. 8. SEM images of PSF with different loadings of GO.

sponge structure. The sub-layer is characterized by the presence of several macro-voids with finger-like structure that have been enlarged and became wider with the GO embedding (Fig. 8). Similar findings have been reported in the literature and can be attributed to the GO hydrophilicity that accelerates the mass-transfer between water and solvent during the NIPS process [54,68,69]. In contrast, no significant enlargement can be observed in the pore structure with the addition of rGO-DDA (Fig. 9), which can be related to its hydrophobic nature as discussed earlier. High magnification SEM images presented in Fig. 10 show that both nanofillers aggregate in some areas of the sublayer and partially clog the membrane pores. This is considered one of the drawbacks of GO embedding in MMMs as this blockage decreases the water permeance across the membrane as elaborated in the following sections.

The membrane separation and antifouling properties are also affected by the surface roughness [70]. Therefore, AFM analysis was employed to investigate the effects of GO and rGO-DDA embedding on the surface roughness. The 3D AFM images over 5 × 5 µm scan area and roughness parameters of the tested membranes are shown in Fig. 11 and Table 3, respectively. The results show a clear increase in the surface roughness with the high concentrations of pristine GO while it remains the same with low concentrations of GO (e.g. 0.02 %). The roughness parameters of the neat PSF were 7.1 and 5.7 nm for RMS and Ra, respectively, that increased up to 16 and 11.5 nm with 0.15 wt.% GO. When comparing PSF and GO-based membranes with rGO-DDA-based membranes, RMS and Ra were found to decrease with rGO-DDA addition indicating that rGO-DDA based membrane were apparently smoother than the neat PSF and GO-based MMMs. It well known that membranes with rough surfaces have higher fouling propensity because of the accumulation of foulants in the surface valleys [67,71], while membranes with smoother surface have higher fouling resistance capability [72].

3.3.3. Hydrophilicity, porosity and mean pore size

Water contact angle (CA) of the prepared membranes was measured to investigate the effect of GO and rGO-DDA embedding on PSF hydrophilicity and is presented in Fig. 12. The results show a slight enhancement in the hydrophilicity with the embedding of pristine GO as the CA decreased from 83.5° with PSF to 75.5° with GO-0.15. The hydrophilicity enhancement with GO addition is attributed to the GO hydrophilicity which was observed and reported in several studies [67,73]. In contrast, rGO-DDA based MMMs exhibited less hydrophilicity than GO based MMMs. The average CA of rGO-DDA based membranes were close to this of the pristine PSF and were in the range of 81.9° - 83.1°. This agrees with the characterization results of rGO-DDA that showed a hydrophobic nature of rGO-DDA compared to unfunctionalized GO.

The effect of GO/rGO-DDA incorporation on the membrane porosity (ε) and mean pore size (R_m) was investigated by the gravimetric method and the measured values of ε and R_m are listed in Table 3. Low dosage of both GO and rGO-DDA (e.g. 0.02 wt.%) increased the porosity of PSF from 81.2 % to about 86.6 % and 86.5 %, respectively. This increase can be attributed to the acceleration of mass-transfer rate between the solvent and the coagulant during the NIPS process as discussed earlier.

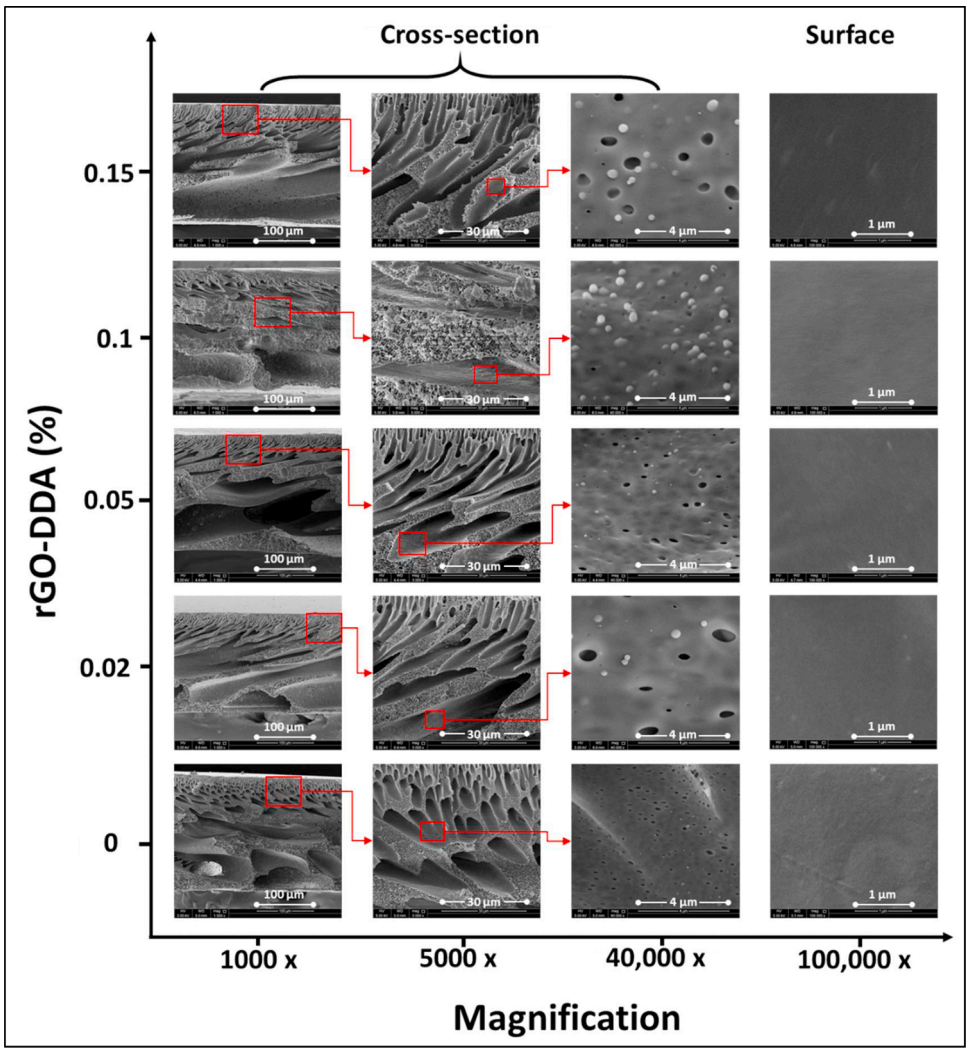

Fig. 9. SEM images of PSF with different loadings of rGO-DDA.

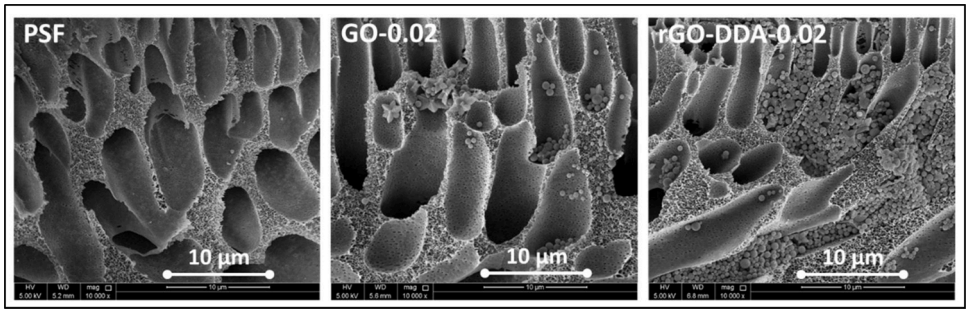

Fig. 10. cross-section SEM images (10,000 x magnification) of PSF, GO-0.02, and rGO-DDA -0.02 showing pores clogging by nanomaterial.

However, when increasing the concentration to 0.15 %, the porosity decreased to 79.9 % and 78.7 % for GO and rGO-DDA, respectively. Excessive compositions of nanofiller increase the dope solution viscosity which slows the mass transfer rate during the NIPS process, lowers the membrane porosity and forms smaller pores [27]. The mean pore size (R_m) of the bare PSF membrane was estimated to be ~37.5 nm and was decreased with the addition of both nanofillers. The estimated R_m values were ranging between 33–36.9 nm and 27.5–36.6 nm with GO and rGO-DDA membranes, respectively. Similar findings were reported in the literature [68,73,74], and can be attributed to the increase in dope solution viscosity accompanied with the accumulation of nanofillers in the pores as revealed by the SEM analysis (Fig. 10).

3.4. Permeability and rejection properties

The performance of the prepared membranes in terms of the pure water permeability (PWP) and rejection is illustrated in Fig. 13. The measured PWP of the neat PSF was 181.7 ± 4.6 $L.m^{-2}.h^{-1}.bar^{-1}$. With low concentration of nanomaterial, no significant change was observed and the measured PWP was 181.1 ± 9.4 and 180.4 ± 4.5 $L.m^{-2}.h^{-1}.bar^{-1}$ for GO-0.02 and rGO-DDA-0.02, respectively. However, with excessive concentrations of the GO and rGO-DDA, membranes exhibited higher

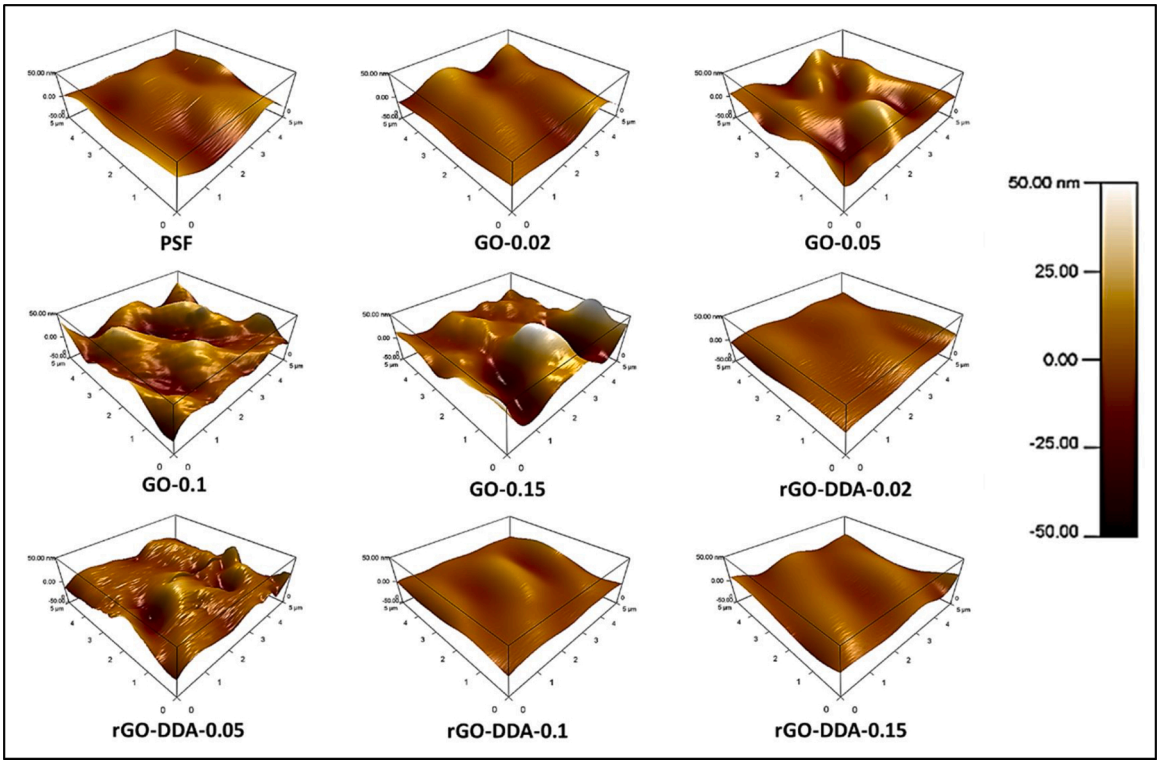

Fig. 11. AFM images of the PSF, GO and rGO-DDA based membranes.

Table 3
The measured roughness parameters (RMS and Ra), porosity (Ɛ) and mean pore size (R_m) of the pristine PSF and composite membranes.

Membrane	RMS (nm)	Ra (nm)	Ɛ (%)	R_m (nm)
PSF	7.1	5.7	81.2 ± 0.1	37.5 ± 0.1
GO-0.02	7.0	5.7	86.6 ± 5.1	33.7 ± 2.1
GO-0.05	9.4	7.4	85.5 ± 0.2	34.4 ± 0.1
GO-0.1	13.2	10.5	82.9 ± 0.1	36.9 ± 0.0
GO-0.15	16.0	11.5	79.9 ± 2.8	33.0 ± 1.1
rGO-DDA-0.02	6.3	5.2	86.5 ± 3.4	32.6 ± 1.2
rGO-DDA-0.05	7.2	5.4	81.1 ± 0.1	36.6 ± 0.1
rGO-DDA-0.1	5.1	4.0	79.8 ± 1.7	36.4 ± 0.8
rGO-DDA-0.15	4.9	4.1	78.7 ± 1.2	27.5 ± 0.4

decreases in PWP. With 0.15 wt.% GO, PWP decreased by approximately 26 % while the decrease was much higher with 0.15 wt.% rGO-DDA (~51 %). The flux decline at high GO concentrations was reported in many studies [35,67,73] and is mainly attributed to the increase in dope solution viscosity [75–77]. As discussed earlier, the increase in viscosity decreases the porosity and the mean pore size and hence decreases the water flux. The filler concentration after which the permeability decreases is generally referred to as the tipping mass percentage that differs depending on the type of polymer and filler [67]. Hence, the findings in this work indicate that the tipping mass percentage of both GO and rGO-DDA is lower than 0.02 wt.%. Further analysis of the PWP results obtained taking into consideration porosity, mean pore size and contact angle measurements shows that PWP decreases as the porosity and pore size decrease regardless the increases in surface hydrophilicity. This observation suggests that porosity and pore size have more impact on permeability compared to surface hydrophilicity which agrees with

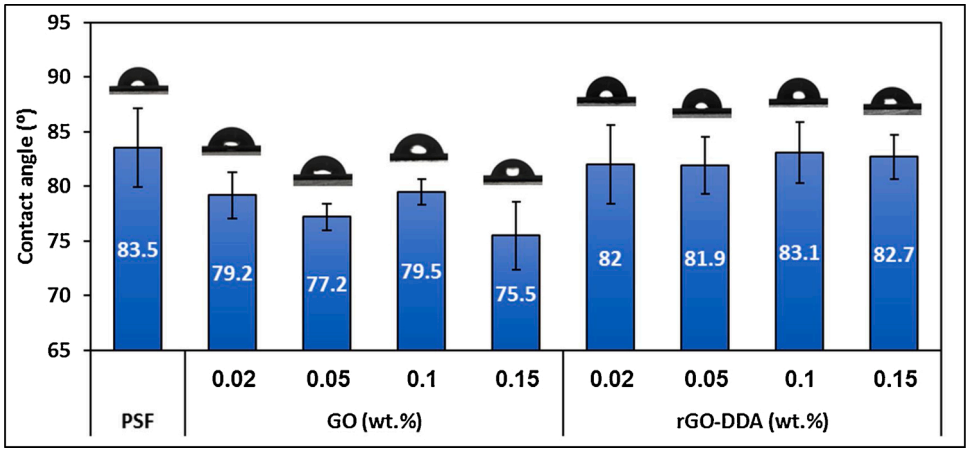

Fig. 12. contact angle of the prepared membranes.

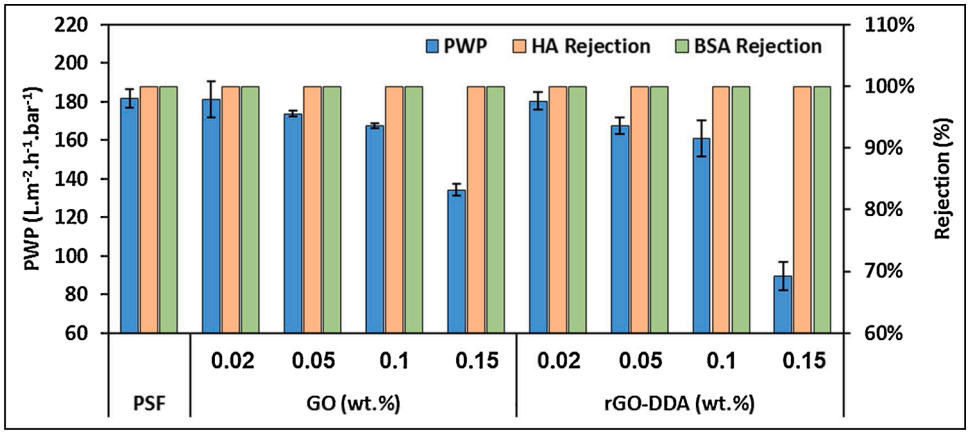

Fig. 13. Separation performance of the prepared membranes.

findings by several studies [67,78,79].

As depicted in Fig. 13, a complete rejection of both HA and BSA was observed with the pristine PSF and all the GO and rGO-DDA composite membranes. Figure S4 in the supplementary information presents photographs of feed and permeate samples taken during HA separation experiments. The high rejection can be mainly linked to main mechanisms: the molecular size exclusion mechanism that retain large molecules like HA and BSA accompanied with the charge-based mechanisms that enhances the electrostatic repulsion of foulant molecules with the negatively charged membranes [38,80]. Similar results were obtained with other GO-based MMMs investigated in the literature like PES/SPSF/GO [80], PSF/GO [67], PSF/GO-PDA [27], PES/CSGO [36], PSF/GOQD [81], and SPES/GO-SiO_2-NH_2 [38].

3.5. Antifouling measurements

The high fouling resistance against various foulants is an essential characteristic of a high-efficient membrane. Fouling is a typical phenomenon associated with the membrane filtration process caused by the concentration polymerization and formation of cake layers that block the membrane pores and reduces the flux and permeate quality [2]. A flux reduction was observed with all the tested membranes when shifting the feed solution from DI to HA or BSA due to the accumulation of foulant molecules on the surface and the formation of cake layers. After 1 h of foulant filtration, the membranes were washed with DI three times (10 min each) and exhibited a partial flux recovery that was accordingly calculated (FRR). The antifouling performance against both foulants (BSA and HA) of the prepared membranes represented by FRR values is depicted in Fig. 14a. Obviously, all GO and rGO-DDA based membranes showed higher FRR compared to this of the neat PSF that exhibited 65.4 % and 87.8 % with BSA and HA, respectively. With BSA as foulant, the FRR% was significantly improved to 81.3, 84.6, 89.1 and 93.7 % with the embedding of 0.02, 0.05, 0.1, and 0.15 wt.% rGO-DDA, respectively. In contrast, the FRR% enhancement with the pristine GO addition was lower and the maximum FRR% was 86.9 % with GO-0.1. When using HA as foulant, the FRR increased up to 97.0 % and 99.3 % with GO-0.15 and rGO-DDA-0.1, respectively. The antifouling properties of the tested membrane were further analyzed by estimating the fouling resistance parameters that are presented in Fig. 14b and c for HA and BSA, respectively. Obviously, the total fouling ratio (R_t) and the irreversible fouling ratio (R_{ir}) of the pristine PSF were higher than these of all modified membranes and vice versa for the reversible fouling ratio (R_r). These results lead to the same conclusion that the modified membranes have higher fouling resistance compared to the neat PSF.

It is well known that the reversible fouling ratio (R_r) of a membrane is highly affected by its surface hydrophilicity and roughness [82]. As confirmed by the AFM analysis, rGO-DDA based membranes have relatively smoother surfaces than PSF and GO-based membranes. Therefore, the accumulation of foulants is restricted and can be washed easily from the surface during the washing cycles. In contrast, GO-based membranes showed higher surface roughness than this of the pristine PSF and rGO-DDA based membranes. Hence, surface roughness enhances the accumulation of foulant molecules in the valleys which cause a significant reduction in the flux during the foulant filtration stage. In the next stage (washing with DI), the hydrophilic nature of GO nanoparticles, distributed on the membrane surface and within the membrane pores, induces the removal and washing of foulants with water [82,83]. Therefore, the fouling resistance was enhanced with GO embedding regardless the high surface roughness, which agrees with some studies in the literature [38,70,84]. Taken together, the findings herein suggest that the fouling resistance of the composite membranes were enhanced by the hydrophilicity in case of the pristine GO addition, and by the lower surface roughness in case of rGO-DDA addition.

Figures S5 and S6 in the supplementary information present SEM images for some fouled membranes at magnification of 10,000 x at two different locations on the surface with BSA and HA, respectively. Figure S7 in the supplementary information shows microphotographs of HA-fouled membranes at two different locations on the surface. Both SEM images and microphotographs confirm the higher fouling resistance of GO and rGO-DDA based MMMs compared to the bare PSF.

3.6. Antibacterial activity measurements

Bacteriostasis rate (BR%) determination is commonly performed to quantitatively evaluate the membranes antibacterial activity [35,55,73]. As depicted in Fig. 15, the number of colonies on the pristine PSF plate indicates no bactericidal effect against *H. aquamarina*. In contrast, the number of colonies was much lower with GO-0.15 and rGO-DDA-0.15 composite membranes suggesting a clear antibacterial activity of both nanoparticles. The lowest number of bacterial colonies was observed with rGO-DDA-0.15 that exhibited an antibacterial rate of 83.6 %, while the antibacterial rate of GO-0.15 was only 62.9 %. Both GO and DDA have bactericidal activity against various bacteria. The bactericidal activity of GO nanosheets is mainly attributed to two mechanisms. The sharp edges of GO sheets cause a physical disruption and damage of the bacterial cells when contacting GO nanoparticles. Additionally, GO induces the oxidative stress on the bacterial cells due to the formation of reactive oxygen species (ROS) [55,85]. Some studies have reported that the oxidative stress is the major antibacterial mechanism of GO-based materials and hence GO possesses an antibacterial effect even if there is no direct contact between the bacterial cells and GO edges [86,87]. The GO bactericidal activity is further enhanced when functionalized with DDA due to the amine functionality that assists the electrostatic interactions between the bacteria and GO

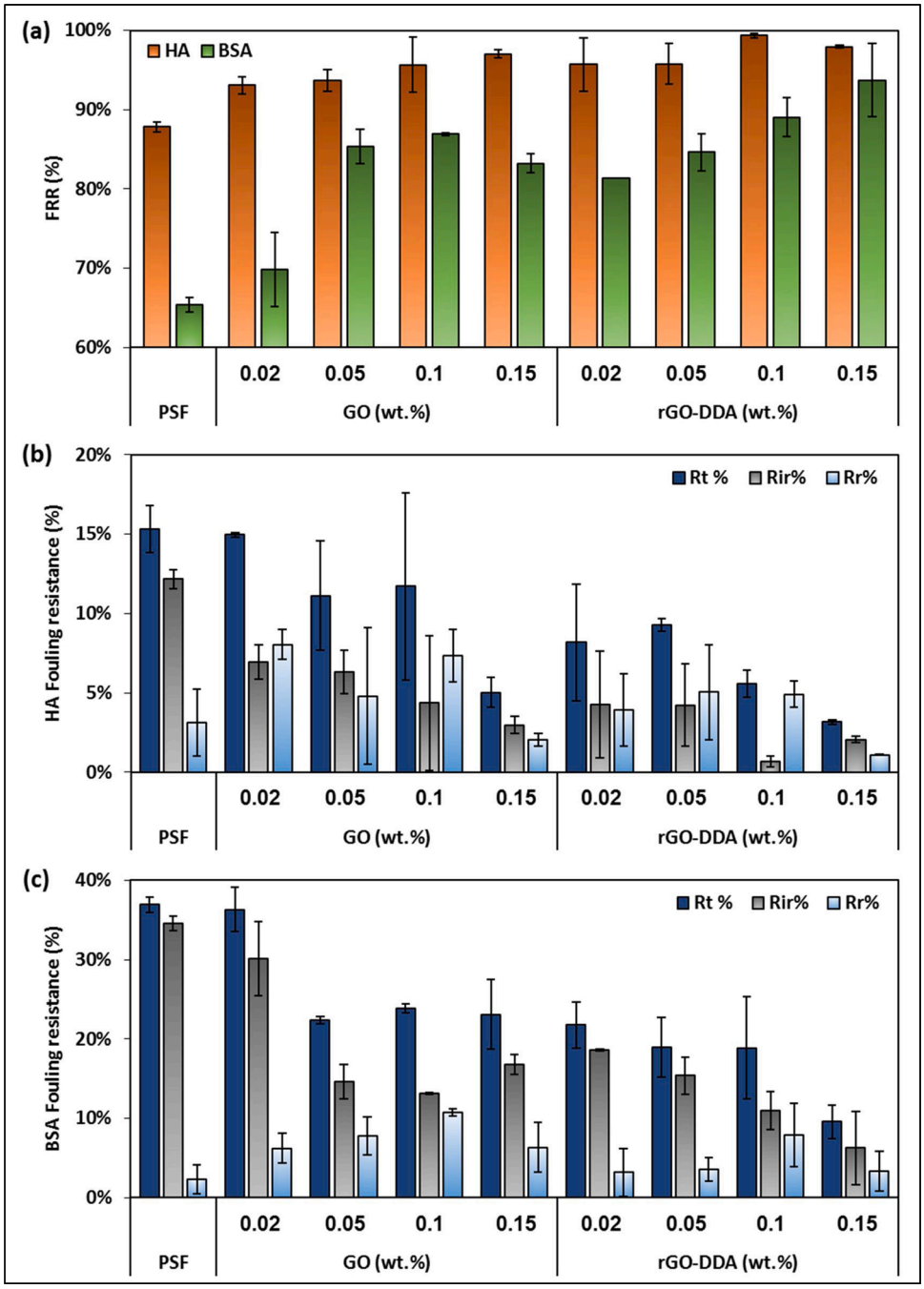

Fig. 14. Antifouling properties of the prepared membranes represented by (a) FRR values after HA and BSA filtration, fouling resistance parameters of (b) HA and (c) BSA.

nanosheets [39]. Therefore, rGO-DDA exhibited a synergetic antibacterial effect against *H. aquamarina* resulting in a higher bacteriostasis rate. Duan et al. [55] prepared PES UF membranes incorporating graphene oxide immobilized lysozyme (GO-Ly) and reduced graphene oxide (CRGO) and reported antibacterial rate of 68 % and 71 %, respectively. Similar work was conducted by Yu et al. [35] by embedding GO-modified by hyperbranched polyethylenimine (HEPI-GO) into PES and reported a bacteriostasis rate of 74.88 %.

It is commonly known that the antibacterial activity of a GO-based material is highly dependent on the topography, roughness, wettability and hydrophobicity of the surface [88,89]. Furthermore, the bacterial adsorption on surfaces with moderate hydrophobicity (contact angle of 45−130°) is stronger than this on hydrophilic surfaces [88–90]. Therefore, the bacterial adsorption on rGO-DDA membranes might be higher than this on GO-based membranes as they have slightly higher hydrophobicity. This implies that DDA increased the adsorption of bacterial cells to GO sheets due to its hydrophobicity along with the amine functionality and hence increased the contact and interactions between them resulting in more physical damage to the microorganisms. Therefore, rGO-DDA-based membranes showed as well as or better antibacterial activity than other GO-based membranes reported in literature. It is worth mentioning that UF membranes are resistant to chlorine that is widely used as disinfectant [2]. However other membrane technologies relying on polyamide materials like RO and NF are not chlorine tolerant, and chlorine must be removed from water before reaching the polyamide membranes. With increasing concerns about chlorine usage in environment and especially the potential formation trihalomethanes which are considered as carcinogenic products, a need

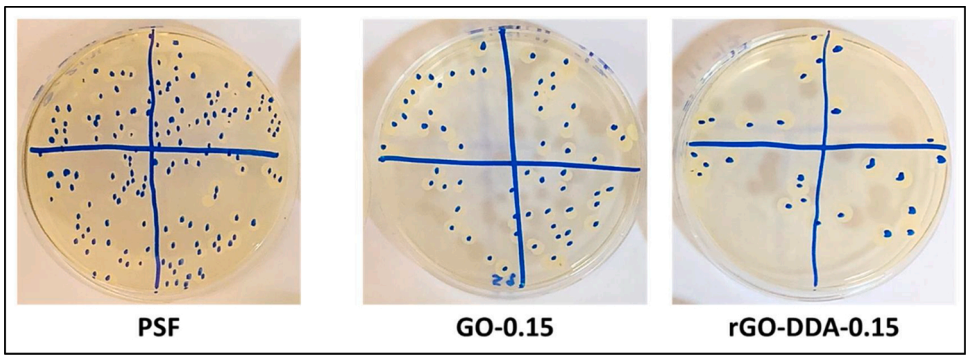

Fig. 15. antibacterial activity observations of pristine PSF, GO-0.15, and rGO-DDA-0.15.

to look for alternatives is a vital issue. Developing new membranes with antibacterial properties offers a good alternative to eliminate or reduce using the disinfectants. GO membranes and functionalized GO membranes are offering such an advantage over using the disinfectants especially when used as a pre-treatment process for NF and RO processes.

Table 4 compares the performance of GO-0.1, GO-0.15, rGO-DDA-0.1 and rGO-DDA-0.15 with other GO-based UF MMMs in literature in terms of PWP, rejection, FRR, and bacteriostasis rate. Most of these membranes were prepared using polyethersulfone (PES) as the main polymeric material while PSF, PVDF, PVC and PEI were used in some studies. Obviously, GO-0.1 and GO-0.15 lies in the range of other GO-based membranes in literature with respect to FRR and rejection. rGO-DDA-0.1 and rGO-DDA-0.15 showed higher FRR against both foulants with pure water flux in the range of other recently reported GO-based membranes. Some literature reported high flux GO-based membranes (>300 L. m^{-2}. h^{-1}. bar^{-1}) [47,70,73,82,91], but these membranes have either low FRR or low rejection.

4. Conclusion

In this work, the potential use of rGO-DDA as membrane nanofiller was investigated. GO nanoparticles were successfully synthesized and functionalized with DDA as revealed by the characterization results and formed rGO-DDA. rGO-DDA was found to have better dispersion properties in several organic solvent. However, it showed poor dispersion in water caused by its hydrophobic nature. The effect of rGO-DDA on the flux, rejection, antifouling, and antibacterial properties of PSF MMMs was also investigated. The incorporation of GO and rGO-DDA was performed via sonication and direct mixing followed by casting using the NIPS technique. Results obtained from membrane characterizations confirmed the successful incorporation of nanoparticles into the polymeric matrix of PSF. The synthesized membranes exhibited different characteristics with respect to morphology, hydrophilicity, porosity and mean pore size. Surface roughness increased with GO addition, while membrane surface became smoother with rGO-DDA addition. Hydrophilicity was also found to increase with GO addition due to its hydrophilic nature. In contrast, due to the hydrophobic characteristics of rGO-DDA, no obvious change on hydrophilicity of PSF was recorded with the addition of rGO-DDA.

Flux and rejection experiments performed in a cross-flow membrane setup revealed that the increase in concentration of both GO and rGO-DDA in the polymeric matrix lead to reduction of the pure water flux. This can be related to the smaller pore size of these membranes as depicted in the mean pore size measurements. All membranes including the bare PSF showed complete rejection of HA and BSA. Antifouling and

Table 4
Comparison of membranes investigated in this work with GO-based UF membranes in literature.

Membrane	Foulant composition (ppm)	PWP (L. m^{-2}. h^{-1}. bar^{-1})	Rejection %	FRR%	BR%	Ref.
Isocyanate-GO/PSF	1000 ppm BSA	135	95	40.27	–	[34]
GO-APTS/PVDF	1000 BSA	401.39	57	95	–	[82]
GO-Ag/PES	500 ppm BSA	143.3	98	67.2	–	[44]
Co_3O_4-GO/PES	1000 ppm BSA	347.9	95	81.1	86.7 (*E. coli*)	[73]
PEI-GO/BPPO	200 ppm BSA	532.5	91	63	–	[70]
GO-PES	10 ppm HA	~ 91	93.9	89.5 ± 7.3	–	[50]
GFG-PSF	200 ppm BSA	217	95.2	82.4	–	[37]
GO-PVC	1000 ppm BSA	430	91.2	70.4	–	[91]
CGO-PSF	1000 ppm BSA	48.8 ± 3.7	100	76.3 ± 17	–	[67]
LIG-GO-PES	1000 ppm BSA	78 ± 7	69 ± 2	91	–	[92]
GO-PES	50 ppm HA	340	95 - 98	80 -95	–	[47]
GO-PSF	1000 ppm BSA	309.2 ± 5.3	–	90.4 ± 2.8	–	[83]
TiO_2-GO-PVDF	1000 ppm BSA	199.97	91.38	89.22	–	[48]
PES/CRGO-Ly	–	372.3	–	–	71 (*E. coli*)	[55]
PSF/GO	–	158	–	–	66 (*E. coli*)	[93]
PES/GO-HPEI	1000 ppm BSA	153.5	–	92.1	74.9 (*E. coli*)	[35]
PES/ZGO-NH	1000 ppm BSA	95.5	95	84.4	81.1 (*E. coli*) 85.7 (*S. aureus*)	[39]
GO-0.1	500 ppm BSA	167.4 ± 1.2	100	BSA: 86.9 ± 0.1 HA: 95.4 ± 4.2	–	This work
GO-0.15	25 ppm HA	134.3 ± 3.2	100	BSA: 83.2 ± 1.2 HA: 97.0 ± 0.5	62.9 (*H. aquamarina*)	
rGO-DDA-0.1		161.0 ± 9.3	100	BSA: 89.1 ± 2.4 HA: 99.3 ± 0.3	–	
rGO-DDA-0.15		89.6 ± 7.1	100	BSA: 93.7 ± 4.6 HA: 97.9 ± 0.2	83.6 (*H. aquamarina*)	

antibacterial properties of the GO-based MMMs were in the range of other GO-based membranes reported in literature. However, rGO-DDA based membranes exhibited superior antifouling and antibacterial properties compared to pristine PSF and GO based membranes. In summary, the functionalization of GO with DDA enhanced GO characteristics and therefore resulted in high-antifouling and antibacterial UF membranes. The utilization of rGO-DDA is not limited to the incorporation with PSF. It has the potential to be used as nanofiller with several polymers due to its ability to be well-dispersed in various organic solvents. Additionally, it can be incorporated as nanofiller in TFN layers to form NF or RO membranes. For example, in interfacial polymerization technique that is commonly used for NF and RO membranes [94], rGO-DDA can be easily incorporated in the organic layer by the dispersion in hexane or dodecane.

Declaration of Competing Interest

The authors declare that they have no known competing financial interests or personal relationships that could have appeared to influence the work reported in this paper.

Acknowledgment

This work was made possible by an Award [GSRA4-1-0504-17043] from Qatar National Research Fund (QNRF, a member of Qatar Foundation). The contents herein are solely the responsibility of the authors. Open access funding is provided by Qatar National Library. Authors would like to thank also the Central Lab Unit (CLU) and Center of Advanced Materials (CAM) in Qatar University (QU) for their support in materials characterization. We also thank Dr. Mohammad Yousaf Ashfaq, Department of Biological & Environmental Sciences of Qatar University, for his support in antibacterial activity measurements.

Appendix A. Supplementary data

Supplementary material related to this article can be found, in the online version, at doi:https://doi.org/10.1016/j.jwpe.2021.102120.

References

[1] H. Abdelrazeq, et al., Performance of electrospun polystyrene membranes in synthetic produced industrial water using direct-contact membrane distillation, Desalination 493 (2020), 114663.
[2] A. Alkhouzaam, H. Qiblawey, Functional GO-based membranes for water treatment and desalination: fabrication methods, performance and advantages, A review, Chemosphere 274 (2021), 129853.
[3] M. Hafiz, et al., Comparison of Nanofiltration with reverse osmosis in reclaiming tertiary treated municipal wastewater for irrigation purposes, Membranes 11 (2021) 32.
[4] Al Aani, S.T.N. Mustafa, N. Hilal, Ultrafiltration membranes for wastewater and water process engineering: a comprehensive statistical review over the past decade, J. Water Process. Eng. 35 (2020), 101241.
[5] M.A. Hafiz, et al., Comparison of dual stage ultrafiltration and hybrid ultrafiltration-forward osmosis process for harvesting microalgae (Tetraselmis sp.) biomass, Chem. Eng. Process. Process. Intensif. 157 (2020), 108112.
[6] M.S. Thabit, et al., Evaluation of forward osmosis as a pretreatment process for multi stage flash seawater desalination, Desalination 461 (2019) 22–29.
[7] P.S. Goh, A.F. Ismail, N. Hilal, Nano-enabled membranes technology: Sustainable and revolutionary solutions for membrane desalination? Desalination 380 (2016) 100–104.
[8] N. Song, et al., A review of graphene-based separation membrane: materials, characteristics, preparation and applications, Desalination 437 (2018) 59–72.
[9] A. Najjar, et al., Antibiofouling performance by polyethersulfone membranes cast with oxidized multiwalled carbon nanotubes and arabic gum, Membranes 9 (2019).
[10] S.F. Anis, et al., Breaking through the selectivity-permeability tradeoff using nano zeolite-Y for micellar enhanced ultrafiltration dye rejection application, Sep. Purif. Technol. 242 (2020), 116824.
[11] M. Samari, et al., Designing of a novel polyethersulfone (PES) ultrafiltration (UF) membrane with thermal stability and high fouling resistance using melamine-modified zirconium-based metal-organic framework (UiO-66-NH2/MOF), Sep. Purif. Technol. 251 (2020), 117010.
[12] M.Y. Ashfaq, et al., Investigating the effect of temperature on calcium sulfate scaling of reverse osmosis membranes using FTIR, SEM-EDX and multivariate analysis, Sci. Total Environ. 703 (2020), 134726.
[13] M.Y. Ashfaq, et al., Effect of concentration of calcium and sulfate ions on gypsum scaling of reverse osmosis membrane, mechanistic study, J. Mater. Res. Technol. 9 (2020) 13459–13473.
[14] B. Saini, M.K. Sinha, S.K. Dash, Mitigation of HA, BSA and oil/water emulsion fouling of PVDF Ultrafiltration Membranes by SiO2-g-PEGMA nanoparticles, J. Water Process. Eng. 30 (2019), 100603.
[15] R. Alfahel, et al., Fabrication of fouling resistant Ti3C2Tx (MXene)/cellulose acetate nanocomposite membrane for forward osmosis application, J. Water Process. Eng. 38 (2020), 101551.
[16] C.N. Matindi, et al., Tailoring the morphology of polyethersulfone/sulfonated polysulfone ultrafiltration membranes for highly efficient separation of oil-in-water emulsions using TiO2 nanoparticles, J. Memb. Sci. 620 (2021), 118868.
[17] A.I. Alkhouzaam, H. Qiblawey, M. Khraisheh, Synthesis of High-antifouling and antibacterial ultrafiltration membranes incorporating Low concentrations of graphene oxide. Qatar University Annual Research Forum and Exhibition (QUARFE 2020), Qatar University Press, Doha, Qatar, 2020.
[18] E. Valamohammadi, et al., Preparation of positively charged thin-film nanocomposite membranes based on the reaction between hydrolyzed polyacrylonitrile containing carbon nanomaterials and HPEI for water treatment application, Sep. Purif. Technol. 242 (2020), 116826.
[19] N.K. Khanzada, et al., Evaluation of anti-bacterial adhesion performance of polydopamine cross-linked graphene oxide RO membrane via in situ optical coherence tomography, Desalination 479 (2020), 114339.
[20] A. Lerf, et al., Structure of graphite oxide revisited, J. Phys. Chem. B 102 (1998) 4477–4482.
[21] S. Stankovich, et al., Graphene-based composite materials, Nature 442 (2006) 282.
[22] P.G. Ren, et al., Characterization and performance of dodecyl amine functionalized graphene oxide and dodecyl amine functionalized graphene/high-density polyethylene nanocomposites: a comparative study, J. Appl. Polym. Sci. 131 (2014).
[23] S. Chakraborty, et al., High yield synthesis of amine functionalized graphene oxide and its surface properties, RSC Adv. 6 (2016) 67916–67924.
[24] Y.-J. Wan, et al., Improved dispersion and interface in the graphene/epoxy composites via a facile surfactant-assisted process, Compos. Sci. Technol. 82 (2013) 60–68.
[25] J. Zahirifar, et al., Fabrication of a novel octadecylamine functionalized graphene oxide/PVDF dual-layer flat sheet membrane for desalination via air gap membrane distillation, Desalination 428 (2018) 227–239.
[26] K.-J. Lu, J. Zuo, T.-S. Chung, Novel PVDF membranes comprising n-butylamine functionalized graphene oxide for direct contact membrane distillation, J. Memb. Sci. 539 (2017) 34–42.
[27] A. Alkhouzaam, H. Qiblawey, Novel polysulfone ultrafiltration membranes incorporating polydopamine functionalized graphene oxide with enhanced flux and fouling resistance, J. Memb. Sci. 620 (2021), 118900.
[28] X. Wu, et al., Polyvinylpyrrolidone modified graphene oxide as a modifier for thin film composite forward osmosis membranes, J. Memb. Sci. 540 (2017) 251–260.
[29] J.P. Ambre, et al., High flux hyperbranched starch-graphene oxide piperazinamide composite nanofiltration membrane, J. Environ. Chem. Eng. 7 (2019), 103300.
[30] M. Safarpour, A. Khataee, V. Vatanpour, Thin film nanocomposite reverse osmosis membrane modified by reduced graphene oxide/TiO2 with improved desalination performance, J. Memb. Sci. 489 (2015) 43–54.
[31] M. Safarpour, et al., Development of a novel high flux and fouling-resistant thin film composite nanofiltration membrane by embedding reduced graphene oxide/TiO2, Sep. Purif. Technol. 154 (2015) 96–107.
[32] R. Rajakumaran, et al., Effect of ZnO morphology on GO-ZnO modified polyamide reverse osmosis membranes for desalination, Desalination 467 (2019) 245–256.
[33] Y. Zhang, et al., Thin-film nanocomposite reverse osmosis membranes with enhanced antibacterial resistance by incorporating p-aminophenol-modified graphene oxide, Sep. Purif. Technol. 234 (2020), 116017.
[34] H. Zhao, et al., Improving the antifouling property of polysulfone ultrafiltration membrane by incorporation of isocyanate-treated graphene oxide, J. Chem. Soc. Faraday Trans. 15 (2013) 9084–9092.
[35] L. Yu, et al., Preparation and characterization of HPEI-GO/PES ultrafiltration membrane with antifouling and antibacterial properties, J. Memb. Sci. 447 (2013) 452–462.
[36] S. Kong, et al., High-flux and antifouling polyethersulfone nanocomposite membranes incorporated with zwitterion-functionalized graphene oxide for ultrafiltration applications, J. Ind. Eng. Chem. 84 (2020) 131–140.
[37] G. Zhang, et al., Guanidyl-functionalized graphene/polysulfone mixed matrix ultrafiltration membrane with superior permselective, antifouling and antibacterial properties for water treatment, J. Colloid Interface Sci. 540 (2019) 295–305.
[38] M. Kumar, et al., High-flux, antifouling hydrophilized ultrafiltration membranes with tunable charge density combining sulfonated poly(ether sulfone) and aminated graphene oxide nanohybrid, ACS Appl. Mater. Interfaces 12 (2020) 1617–1627.
[39] N. Ahmad, et al., Enhanced performance and antibacterial properties of amine-functionalized ZIF-8-decorated GO for ultrafiltration membrane, Sep. Purif. Technol. 239 (2020), 116554.
[40] A. Khalid, et al., Preparation and properties of nanocomposite polysulfone/multi-walled carbon nanotubes membranes for desalination, Desalination 367 (2015) 134–144.
[41] G.G. Meynell, Dodecylamine in the isolation of bacterial DNA, Biochimica et Biophysica Acta (BBA) - Nucleic Acids and Protein Synthesis 240 (1971) 37–38.

[42] F.V. Ferreira, et al., Dodecylamine functionalization of carbon nanotubes to improve dispersion, thermal and mechanical properties of polyethylene based nanocomposites, Appl. Surf. Sci. 410 (2017) 267–277.
[43] A. Alkhouzaam, et al., Synthesis of graphene oxides particle of high oxidation degree using a modified Hummers method, Ceram. Int. 46 (2020) 23997–24007.
[44] V. Vatanpour, et al., Fabrication and characterization of anti-fouling and anti-bacterial Ag-loaded graphene oxide/polyethersulfone mixed matrix membrane, J. Ind. Eng. Chem. 30 (2015) 342–352.
[45] X. Chang, et al., Exploring the synergetic effects of graphene oxide (GO) and polyvinylpyrrodione (PVP) on poly(vinylylidenefluoride) (PVDF) ultrafiltration membrane performance, Appl. Surf. Sci. 316 (2014) 537–548.
[46] A. Alkhouzaam, et al., High-pressure CO 2/N 2 and CO 2/CH 4 separation using dense polysulfone-supported ionic liquid membranes, J. Nat. Gas Sci. Eng. 36 (2016) 472–485.
[47] M.S. Algamdi, et al., Fabrication of graphene oxide incorporated polyethersulfone hybrid ultrafiltration membranes for humic acid removal, Sep. Purif. Technol. 223 (2019) 17–23.
[48] L.-g. Wu, et al., Enhanced performance of polyvinylidene fluoride ultrafiltration membranes by incorporating TiO2/graphene oxide, Chem. Eng. Res. Des. 141 (2019) 492–501.
[49] T. Wang, et al., Novel methodology for facile fabrication of nanofiltration membranes based on nucleophilic nature of polydopamine, J. Memb. Sci. 511 (2016) 65–75.
[50] K.H. Chu, et al., Evaluation of graphene oxide-coated ultrafiltration membranes for humic acid removal at different pH and conductivity conditions, Sep. Purif. Technol. 181 (2017) 139–147.
[51] J. Tian, et al., Effect of membrane fouling on chiral separation, J. Memb. Sci. 593 (2020), 117352.
[52] A. Rahimi, H. Mahdavi, Zwitterionic-functionalized GO/PVDF nanocomposite membranes with improved anti-fouling properties, J. Water Process. Eng. 32 (2019) 100960.
[53] T. Wang, et al., Fabrication of high flux nanofiltration membrane via hydrogen bonding based co-deposition of polydopamine with poly(vinyl alcohol), J. Memb. Sci. 552 (2018) 222–233.
[54] V. Vatanpour, et al., Fabrication and characterization of novel antifouling nanofiltration membrane prepared from oxidized multiwalled carbon nanotube/polyethersulfone nanocomposite, J. Memb. Sci. 375 (2011) 284–294.
[55] L. Duan, et al., Graphene immobilized enzyme/polyethersulfone mixed matrix membrane: enhanced antibacterial, permeable and mechanical properties, Appl. Surf. Sci. 355 (2015) 436–445.
[56] J. Guerrero-Contreras, F. Caballero-Briones, Graphene oxide powders with different oxidation degree, prepared by synthesis variations of the Hummers method, Mater. Chem. Phys. 153 (2015) 209–220.
[57] T.T. Nguyen, et al., Effects of grafting methods for functionalization of graphene oxide by dodecylamine on the physical properties of its polyurethane nanocomposites, J. Memb. Sci. 540 (2017) 108–119.
[58] M. Akbari, et al., Janus graphene oxide nanosheet: a promising additive for enhancement of polymeric membranes performance prepared via phase inversion, J. Colloid Interface Sci. 527 (2018) 10–24.
[59] S.E. Lowe, et al., The role of electrolyte acid concentration in the electrochemical exfoliation of graphite: mechanism and synthesis of electrochemical graphene oxide, Int. J. Green Nanotechnol. Mater. Sci. Eng. (2019).
[60] S. Claramunt, et al., The importance of Interbands on the interpretation of the raman Spectrum of graphene oxide, J. Phys. Chem. C 119 (2015) 10123–10129.
[61] A. Alkhouzaam, H. Qiblawey, M. Khraisheh, Polydopamine functionalized graphene oxide as membrane nanofiller: spectral and structural studies, Membranes 11 (2021) 86.
[62] S. Li, et al., Thermal performance and shape-stabilization of comb-like polymeric phase change materials enhanced by octadecylamine-functionalized graphene oxide, Energy Convers. Manage. 168 (2018) 119–127.
[63] M. Bera, A. Prabhakar, P.K. Maji, Nanotailoring of thermoplastic polyurethane by amine functionalized graphene oxide: effect of different amine modifier on final properties, Compos. Part B Eng. 195 (2020), 108075.
[64] N. Yadav, B. Lochab, A comparative study of graphene oxide: hummers, intermediate and improved method, FlatChem 13 (2019) 40–49.
[65] M. Khraisheh, et al., Characterization of polysulfone/diisopropylamine 1-alkyl-3-methylimidazolium ionic liquid membranes: high pressure gas separation applications, Greenh. Gases Sci. Technol. 10 (2020) 795–808.
[66] Y. Kang, et al., Novel sulfonated graphene oxide incorporated polysulfone nanocomposite membranes for enhanced-performance in ultrafiltration process, Chemosphere 207 (2018) 581–589.
[67] Y. Jiang, et al., Graphene oxides as nanofillers in polysulfone ultrafiltration membranes: shape matters, J. Memb. Sci. 581 (2019) 453–461.
[68] S. Zinadini, et al., Preparation of a novel antifouling mixed matrix PES membrane by embedding graphene oxide nanoplates, J. Memb. Sci. 453 (2014) 292–301.
[69] J. Zhang, et al., Synergetic effects of oxidized carbon nanotubes and graphene oxide on fouling control and anti-fouling mechanism of polyvinylidene fluoride ultrafiltration membranes, J. Memb. Sci. 448 (2013) 81–92.
[70] L. Yang, B. Tang, P. Wu, UF membrane with highly improved flux by hydrophilic network between graphene oxide and brominated poly(2,6-dimethyl-1,4-phenylene oxide), J. Mater. Chem. A 2 (2014) 18562–18573.
[71] J. Zhang, et al., Improved hydrophilicity, permeability, antifouling and mechanical performance of PVDF composite ultrafiltration membranes tailored by oxidized low-dimensional carbon nanomaterials, J. Mater. Chem. A 1 (2013) 3101–3111.
[72] L.-Y. Yu, et al., Preparation and characterization of PVDF–SiO2 composite hollow fiber UF membrane by sol–gel method, J. Memb. Sci. 337 (2009) 257–265.
[73] G. Ouyang, et al., Remarkable permeability enhancement of polyethersulfone (PES) ultrafiltration membrane by blending cobalt oxide/graphene oxide nanocomposites, RSC Adv. 5 (2015) 70448–70460.
[74] S. Xia, M. Ni, Preparation of poly(vinylidene fluoride) membranes with graphene oxide addition for natural organic matter removal, J. Memb. Sci. 473 (2015) 54–62.
[75] S. Ayyaru, Y.-H. Ahn, Application of sulfonic acid group functionalized graphene oxide to improve hydrophilicity, permeability, and antifouling of PVDF nanocomposite ultrafiltration membranes, J. Memb. Sci. 525 (2017) 210–219.
[76] N. Meng, et al., The effect of reduction degree of GO nanosheets on microstructure and performance of PVDF/GO hybrid membranes, J. Memb. Sci. 501 (2016) 169–178.
[77] H. Sun, B. Tang, P. Wu, Development of hybrid ultrafiltration membranes with improved water separation properties using modified superhydrophilic metal–Organic framework nanoparticles, ACS Appl. Mater. Interfaces 9 (2017) 21473–21484.
[78] J.-F. Li, et al., Effect of TiO2 nanoparticles on the surface morphology and performance of microporous PES membrane, Appl. Surf. Sci. 255 (2009) 4725–4732.
[79] A. Razmjou, J. Mansouri, V. Chen, The effects of mechanical and chemical modification of TiO2 nanoparticles on the surface chemistry, structure and fouling performance of PES ultrafiltration membranes, J. Memb. Sci. 378 (2011) 73–84.
[80] M. Hu, et al., Ultra-low graphene oxide loading for water permeability, antifouling and antibacterial improvement of polyethersulfone/sulfonated polysulfone ultrafiltration membranes, J. Colloid Interface Sci. 552 (2019) 319–331.
[81] G. Zhao, et al., Graphene oxide quantum dots embedded polysulfone membranes with enhanced hydrophilicity, permeability and antifouling performance, Sci. China Mater. 62 (2019) 1177–1187.
[82] Z. Xu, et al., Organosilane-functionalized graphene oxide for enhanced antifouling and mechanical properties of polyvinylidene fluoride ultrafiltration membranes, J. Memb. Sci. 458 (2014) 1–13.
[83] T. Hwang, et al., Ultrafiltration using graphene oxide surface-embedded polysulfone membranes, Sep. Purif. Technol. 166 (2016) 41–47.
[84] S. Ayyaru, T.T.L. Dinh, Y.-H. Ahn, Enhanced antifouling performance of PVDF ultrafiltration membrane by blending zinc oxide with support of graphene oxide nanoparticle, Chemosphere 241 (2020), 125068.
[85] Y. Jiang, et al., Engineered crumpled graphene oxide nanocomposite membrane assemblies for advanced water treatment processes, Environ. Sci. Technol. 49 (2015) 6846–6854.
[86] P. Kumar, et al., Antibacterial properties of graphene-based nanomaterials, Nanomaterials (Basel) 9 (2019) 737.
[87] S. Romero-Vargas Castrillón, et al., Interaction of graphene oxide with bacterial cell membranes: insights from force spectroscopy, Environ. Sci. Technol. Lett. 2 (2015) 112–117.
[88] S. Szunerits, R. Boukherroub, Antibacterial activity of graphene-based materials, J. Mater. Chem. B 4 (2016) 6892–6912.
[89] S. Achinas, N. Charalampogiannis, G.J.W. Euverink, A brief recap of microbial adhesion and biofilms, Appl. Sci. 9 (2019) 2801.
[90] Y. Yuan, et al., Surface characteristics influencing bacterial adhesion to polymeric substrates, RSC Adv. 7 (2017) 14254–14261.
[91] Y. Zhao, et al., Performance enhancement of polyvinyl chloride ultrafiltration membrane modified with graphene oxide, J. Colloid Interface Sci. 480 (2016) 1–8.
[92] A.K. Thakur, et al., Graphene oxide on laser-induced graphene filters for antifouling, electrically conductive ultrafiltration membranes, J. Memb. Sci. 591 (2019), 117322.
[93] V. Mokkapati, et al., Membrane properties and anti-bacterial/anti-biofouling activity of polysulfone-graphene oxide composite membranes phase inversed in graphene oxide non-solvent, RSC Adv. 7 (2017) 4378–4386.
[94] D.H.N. Perera, et al., Regulating the aqueous phase monomer balance for flux improvement in polyamide thin film composite membranes, J. Memb. Sci. 487 (2015) 74–82.